Published in final edited form as:
Biomaterials. 2008 October ; 29(30): 4091–4099. doi:10.1016/j.biomaterials.2008.06.030.

Microporous Nanofibrous Fibrin-based Scaffolds for Bone Tissue Engineering

Thanaphum Osathanon[†,††], **Michael L. Linnes**[††], **Rupak M. Rajachar**[††], **Buddy D. Ratner**[††], **Martha J. Somerman**[†,†††], and **Cecilia M. Giachelli**[†,††,*]

†*Department of Oral Biology, School of Dentistry, University of Washington, Seattle, WA, 98195.*

††*Department of Bioengineering, College of Engineering, University of Washington, Seattle, WA, 98195.*

†††*Department of Periodontics, School of Dentistry, University of Washington, Seattle, WA, 98195.*

Abstract

The fibrotic response of the body to synthetic polymers limits their success in tissue engineering and other applications. Though porous polymers have demonstrated improved healing, difficulty in controlling their pore sizes and pore interconnections has clouded the understanding of this phenomenon. In this study, a novel method to fabricate natural polymer/calcium phosphate composite scaffolds with tightly controllable pore size, pore interconnection, and calcium phosphate deposition was developed. Microporous, nanofibrous fibrin scaffolds were fabricated using sphere-templating methods. Composite scaffolds were created by solution deposition of calcium phosphate on fibrin surfaces or by direct incorporation of nanocrystalline hydroxyapatite (nHA). The SEM results showed that fibrin scaffolds exhibited a highly porous and interconnected structure. Osteoblast-like cells, obtained from murine calvaria, attached, spread and showed a polygonal morphology on the surface of the biomaterial. Multiple cell layers and fibrillar matrix deposition were observed. Moreover, cells seeded on mineralized fibrin scaffolds exhibited significantly higher alkaline phosphatase activity as well as osteoblast marker gene expression compared to fibrin scaffolds and nHA incorporated fibrin scaffolds (0.25 g and 0.5 g). All types of scaffolds were degraded both *in vitro* and *in vivo*. Furthermore, these scaffolds promoted bone formation in a mouse calvarial defect model and the bone formation was enhanced by addition of rhBMP-2.

Introduction

Existing treatments for large bone defects are limited and often associated with undesirable outcomes [1]. Composite biomaterials containing calcium phosphate and natural or synthetic polymers have been developed to address these limitations. Mineralized collagen was able to promote bone healing at 52 weeks in a rat calvarial defect model [2]. However, the mineralized collagen had very low porosity and no interconnected pores, impeding the migration of surrounding cells into the wound site and delaying bone regeneration. Composite biomaterials consisting of calcium phosphate and synthetic polymers, poly (lactide-co-glycolide) and poly glycolic acid, have been proposed as alternative composite biomaterials for bone regeneration because of the ability to fabricate porous scaffolds with controlled structure and to incorporate

*Corresponding author: Cecilia M. Giachelli, Bioengineering Dept, Box 351720, Foege Hall, Room 330L, University of Washington, Seattle, WA 98192, Phone: 206-543-0205, Fax: 206-616-9763, Email: ceci@u.washington.edu.

calcium phosphate mineral crystals [3]. However, the toxicity of the acidic degradation products of poly (lactide-co-glycolide) has limited their potential uses in bone tissue engineering [4].

Fibrin is a candidate polymer for use in fabricating composite biomaterials for bone regeneration. Fibrin is a natural polymer known to support wound healing by inducing angiogenesis and promoting cell attachment and proliferation [5–7], and thus may provide a more conductive environment for accelerated bone regeneration. Also, for sub-critical defects in bone, the gap is seen to fill with clot and to regenerate to new bone. Several studies have used fibrin sealant as a component for bone regenerative materials [8–10]. However, the dense and low porosity structures produced by fibrin sealant were found to impede cell invasion causing delayed wound healing [9].

We have developed a novel composite calcium phosphate/ fibrin-based scaffold with well-controlled porous architecture for bone regeneration. The aims of this study were to generate porous scaffolds with a uniform, defined pore structure, characterize the chemical and structural properties of these scaffolds and investigate their biological performance *in vitro* and *in vivo*.

Materials and Methods

Fibrin scaffold preparation

Microporous, nanofibrous fibrin scaffolds (FS) (~200–250 μm pore size) were fabricated using a sphere-templating and leaching methods as describe previously [11]. Briefly, poly(methyl methacrylate) (PMMA) (Polysciences, Inc.) beads were sieved to select a 200–250 μm size fraction. The sieved PMMA beads were close-packed using vibration and sintered at 140°C for 22 h. Bovine fibrinogen (Sigma) was dissolved in 0.9% NaCl solution at a concentration of 200 mg/mL and cast to surround PMMA bead templates. Fibrin formation was initiated by adding a bovine thrombin (Sigma) solution (267 U of thrombin in 2.67 mL, 133 μl of 2N $CaCl_2$, 17.2 mL of Dulbecco's Modified Eagle's Medium (DMEM; Gibco)), and incubated for 24 h at room temperature. Finally, the PMMA templates were dissolved in several rinses of acetone over 72 hours and the scaffolds resolvated in 70% ethanol overnight.

Calcium phosphate containing composite scaffolds were generated by two procedures. For mineralized fibrin scaffolds (MFS), the FS scaffolds were incubated in a solution containing 2.5 mM $CaCl_2$-$2H_2O$, 4.2 mM $NaHCO_3$, 146 mM NaCl, and 1 mM K_2HPO_4 at 37°C as modified from Tarasevich B, et al [12]. The solution was changed daily. For hydroxyapatite containing fibrin scaffolds (nHA/FS), 0.25 g or 0.5 g nHA (Berkeley Advanced Biomaterials, CA) was mixed with fibrinogen solution before casting into PMMA templates, and then processed as for FS scaffolds above.

Scanning electron microscope (SEM) analysis

The scaffolds were dehydrated using ascending grades of ethanol and critical point dried. For cell-seeded scaffolds, samples were fixed with 2% glutaraldehyde (Sigma) at room temperature for 1 h before dehydration. All samples were sputter coated with Au/Pd and then examined with SEM (FEI Sirion SEM) at accelerating voltage of 10 kV. The chemical composition of scaffolds was determined using energy dispersive x-ray analysis. The EDX spectra were randomly recorded in five areas in each sample (n=3).

Raman spectroscopic analysis

The Raman spectra of scaffolds were obtained using a Reinshaw in Via Raman microscope (Reinshaw, UK) at a laser excitation wavelength, 785 nm. The laser beam was focused using

Leica 50X objective (numerical aperture: 0.80, working distance: 0.5 mm, spot size <2μm). The spectra were focused on the phosphate's internal mode, the 400–1100 Δcm^{-1} range.

Dissolution experiments

FS, MFS, 0.25 g and 0.5 g nHA/FS scaffolds were incubated in PBS at 37°C up to 56 day. The supernatants were collected and a calcium assay, described below, was employed to determine the solubilized calcium content.

Cell isolation and culture

Primary calvarial cells were isolated from parietal bone of newborn C57/BL6 mice using methods described previously by Kim SS, et al [3]. The calvarial cells from fraction 3–6 [13, 14] were pooled and cultured in growth medium (DMEM (Gibco) supplemented with 1% Penicillin-streptomycin (PS; Gibco), and 10% Fetal bovine serum (FBS; Gibco)) and maintained in humidified 95%, 5% (v/v) CO_2 at 37°C. The medium was changed every 48 h. The cells from passage 2–4 were used in the experiments.

For macrophage preparations, marrow cells were isolated from the femoral marrow cavity of C57/BL6 mice by flushing with RPMI 1640 (Gibco BRL, Carlsbad, CA) culture medium. Dispersed marrow cells were expanded and differentiated in supplemented media (50% RPMI 1640 (RPMI), 30% fibroblastic cell (L929) conditioned medium (L929-CM), and 20% fetal bovine serum (FBS)) for three days. These macrophage cultures were maintained in a minimal media formulation (70% RPMI, 20% L929-CM, and 10% FBS) and media were changed every three days until confluent.

Scaffolds (8 mm in diameter, 1.2 mm in thickness) were sterilized using 70% ethanol, followed by washing in phosphate buffered saline (PBS). 50 μl aliquots of calvarial cell suspension (2×10^6 cells/mL) were seeded on the top surface of scaffolds and cells were allowed to attach for 30 min before adding 500 μl of growth medium. At 24 h, the scaffolds were transferred to fresh plates and medium was changed to osteogenic medium; DMEM supplement with 1% PS, 10% FBS, 10 mM β-glycerophosphate (Sigma), 50 μl/mL L-ascorbic acid (Sigma) and 100 nM dexamethasone (Sigma).

For in vitro degradation studies, bone marrow-derived macrophage cells were seeded on the scaffolds at density of 5×10^5 cells/scaffolds. Scaffolds were cultured in growth medium supplemented with 25 ng/mL macrophage-colony stimulating factor (M-CSF) and 40 ng/mL receptor activator of nuclear factor κB ligand (sRankL) to initiate osteoclast formation. For co-culture, bone marrow-derived macrophages were seeded on the scaffolds after plating the primary calvarial cells for 30 min. The co-cultured cells were maintained in osteogenic medium with M-CSF and sRankL supplement. The media were changed every three days and assays were terminated at day 14.

Cytotoxicity assessment

An indirect cytotoxicity test was performed using an elution method as describe previously [11]. NIH 3T3 cells were plated at 25,000 cells/wells in 96-well plates and maintained in humidified 95%, 5% (v/v) CO_2 at 37°C. At 24 h, the medium was removed and cells were rinsed twice with PBS. The 25%, 50%, 75% and 100% of scaffold's extraction medium (500 μl) was added to the cells. At 24 and 48 h, cell morphology was examined using phase contrast microscopy. Cell viability was evaluated using an MTT assay.

Proliferation study

Cell proliferation was determined using an MTT assay. At designated time points (1, 3, and 7 d), scaffolds seeded with calvarial cells were transferred into new 48 well plates and rinsed

twice with PBS. Fresh culture medium with MTT (Sigma; 0.5 mg/mL) was added and MTT assay was performed. Total cell number was calculated using a standard curve of absorbance versus cell number.

Alkaline phosphatase activity assay

Alkaline phosphatase activity was determined using *p*-nitrophenol phosphate (Sigma) as the substrate. Scaffolds seeded with calvarial cells were rinsed twice with PBS. Cells were lysed in alkaline lysis buffer, followed by three freeze-thaw cycles at - 70°C and 37°C. The aliquots were incubated in glycine buffer containing 2 mg/mL *p*-nitrophenol phosphate. After 30 min, 3N NaOH was added to stop the reaction. The presence of p-nitrophenol was measured at absorbance 405 nm. Total cellular protein was determined using a micro-BCA assay (Bio-Rad). The enzyme activity was normalized to total cellular protein.

Calcium assay

The scaffolds were washed with PBS, snap frozen in liquid nitrogen, and lyophilized. The dry weight of the scaffolds was recorded. Calcium within the scaffolds was solubilized in 0.6 N HCl at 37°C for 24 h. Calcium content of the supernatant was determined using cresophthalein complexone (Teco Diagnostics). The absorbance of samples was measured at 575 nm. The calcium concentration was calculated using a standard curve and normalized to dry weight.

RNA isolation and RT-PCR

Scaffolds seeded with calvarial cells were collected at days 14 and 21 and were preserved in RNAlater (Ambicon, TX). Scaffolds were then pulverized and total RNA extracted using Trizol reagent (Invitrogen), following the instructions provided. RNA (1 μg) was used to synthesize first strand cDNA by reverse transcriptase (Invitrogen). For the polymerase chain reaction, aliquots of synthesized cDNA were added to PCR mixtures containing Taq polymerase (Sigma) and cycled on a DNA thermal cycler. Primers for PCR were as follows: 1) Alkaline phosphatase (ALP) fwd 5′ GCCCTCTCCAAGACATATA 3′, ALP rev 5′ CCATGATCACGTCGATATCC 3′, 2) Bone sialoprotein (BSP) fwd 5′ GAGCCAGGACTGCCGAAAGGAA 3′, BSP rev 5′ CCGTTGTCTCCTCCGCTGCTGC 3′, 3) Collagen type I (COL I) fwd 5′ GAGGCATAAAGGGTCATCGTGG 3′, COL I rev 5′ CATTAGGCGCAGGAAGGTCAG 3′, 4) Osteocalcin (OCN) fwd 5′ CAGCTTGGTGCACACCTAGC 3′, OCN rev 5′ AGGGTTAAGCTCACACTGCTCC 3′ 5) Core binding factor I (CBFA1) fwd 5′ CGCATTCCTCATCCCAGTAT 3′, CBFA1 rev 5′ GGTGGCAGTGTCATCATCTG 3′, 6) Osterix (OSX) fwd 5′ GATGGCGTCCTCTCTGCTTGA 3′, OSX rev 5′ GGGTTAAGGGGAGCAAAGTCAGAT 3′, 7) GAPDH fwd 5′ ACCACAGTCCATGCCATCAC 3′, GAPDH rev 5′ TCCACCACCCTGTTGCTGTA 3′. PCR products were then electrophoresed on a 1.2% agarose gel and visualized by ethidium bromide fluorostaining. The density of bands was determined using densitometry and ImageJ software.

Scaffold preparation for in vivo experiments

Disc-shaped scaffolds 8 mm in diameter and 1.2 mm thick were employed in subcutaneous implantation studies. For mouse calvarial defect experiments, disc-shaped scaffolds 5 mm in diameter and 0.5 mm thick were utilized. Endotoxin testing was performed for all scaffolds prior to implantation. In some experiments, 1 μg carrier free rhBMP-2 (R&D system) in 10 μl sterile PBS was added to the top of the scaffolds immediately prior to implantation.

Subcutaneous implantation and mouse calvarial defect studies

The protocols were approved by IACUC, University of Washington. C57/BL6 mice were anesthetized by an intraperitoneal injection of xylazine and ketamine cocktail. To determine

the *in vivo* compatibility and degradation of these scaffolds, twenty-three, 6–7-week-old mice were used. Scaffolds were implanted into subcutaneous pockets in the dorsal thoracic region. Mice were euthanized and the scaffolds, at day 14 and 30, were removed and prepared for histological analyses.

The mouse calvarial defect model has been employed to study bone healing and regeneration [15–17]. In brief, the calvarial defects were created in 6–7-weeks-old mice under general anesthesia using xylazine and ketamine. Full thickness skin flaps were raised and the left and right parietal bone were exposed. 5 mm diameter defects in parietal bones were generated using a hand drill trephine burr for consistency. Constant saline irrigation was conducted during the procedure. One implant was placed into each bony defect. The skin was resealed. The procedure was performed under sterile conditions. At 45 days, animals were sacrificed by intraperitoneal nembutal injection. A total of 23 mice were used. The mice were divided into groups as follows: a) Empty defect controls (n=4), b) FS alone (n=3), c) MFS alone (n=3), d) nHA/FS alone (n=4), e) FS+rhBMP-2 (n=3), f) MFS+rhBMP-2 (n=4), g) nHA/FS+rhBMP-2 (n=2).

Histological analyses

Tissues were fixed with 10% buffered formalin for 24 h at 4°C. Tissues were then decalcified in acid formalin solution (4% formalin, 10% acetic acid solution) for 1 month at 4°C. The samples were dehydrated in graded alcohol and embedded in paraffin. 5 μm sections were stained with H&E and Masson Trichrome (Sigma) for morphology evaluation. Tartrate resistant acid phosphatase (TRAP) staining was performed according manufacturing protocol (Sigma 387-A). Bone regeneration of these histological sections were scored by an individual blinded to the identity of sections, using a modification of the visual scoring method of Mankani M, et al (Table 1) [18].

Statistical analyses

The data are expressed as mean±standard deviation (SD). Statistical significance was assessed by analysis of variance (ANOVA) followed by Tukey post hoc test. For the bone regeneration score, the Mann-Whitney U test was used to compare empty defects and treatment groups. Differences at $p<0.05$ were considered to be statistically significant.

Results

Characterization of minerals in fibrin-based scaffolds

SEM—Consistent with previous findings [11], the sphere-templating and leaching fabrication methods used here led to the formation of nanofibrillar FS with tightly controlled pore sizes and interconnections. We previously estimated interconnected neck size of the scaffolds to be 50% and the overall porosity of the scaffolds calculated to be 73.7±0.6% as determined by digital volumetric imaging [11]. As shown in Fig 1Aa, FS exhibited a homogeneous, well-interconnected, highly porous structure by SEM. Mineral crystals were observed on the surface as well as the inner walls of the MFS (Fig. 1Ab, 1Ac, and 1Ad). In contrast, in nHA/FS, mineral crystals were embedded throughout the scaffold walls (Fig. 1Ae).

The total mineralization increased corresponding to the incubation period in saturated calcium phosphate solution as shown in Fig. 1Ab–Ad. According to the calcium assay, there was a statistically significant difference ($p<0.05$) in calcium content between scaffolds incubated in saturated calcium phosphate solution for 72 h, 96 h, 7 d, and 14 d compared to those incubated in PBS for 14 d (Figure. 1B). As expected, a significant difference in calcium content between the 0.25 nHA/FS and 0.5 nHA/FS scaffolds was also observed (Figure. 1C).

At higher magnification, the FS incubated in PBS exhibited a fibrillar wall ultrastucture with no mineral crystals observed (Fig. 1Af). MFS scaffolds, Fig. 1Ag, 1Ah, and 1Ai, showed the crystal structure of precipitated minerals on MFS. At early time points, the crystals were coarse. With increasing incubation time, the mineral matured into densely packed, fine crystals. As shown in Fig. 1Aj, nHA/FS scaffolds contained HA crystals packed together and embedded in the polymerized fibrin matrix and/or surrounded by fibrillar fibrin.

EDX—EDX spectra were obtained to determine the chemical compositions of the scaffolds. Carbon (C), nitrogen (N), oxygen (O), sodium (Na), calcium (Ca), and phosphate (P) were detected in MFS and nHA/FS. The Ca/P ratio of MFS was 1.09–2.62 at 24 h and 1.00–1.70 at 14 d after incubation in saturated calcium phosphate solution (Table.2). The observed range of Ca/P ratio decreased with increasing time of incubation, and suggested that dicalcium phosphate dihydrate (Ca/P ratio = 1.00) [19] and octacalcium phosphate (Ca/P ratio = 1.33) [19,20], were the primary calcium phosphate phases present after short term incubation (24–72 h). Additionally, Ca-enrichment was observed by 24 h, suggesting the presence of calcium carbonate, calcium hydroxide or calcium-rich calcium phosphate crystals. At later time points, the Ca/P ratio of MFS indicated the presence of dicalcium phosphate dihydrate and octacalcium phosphate as well as hydroxyapatite (Ca/P ratio = 1.67) [19,20]. The Ca/P ratio of 0.25 g and 0.5 g nHA/FS were 1.33–1.65 and 1.34–1.69, respectively, as expected for hydroxyapatite and octacalcium phosphate.

Raman Spectroscopy

Raman spectroscopy was performed to confirm the composition and structure of the mineral phase on the scaffolds (Fig. 2). Prominent peaks in the region from 400 to 1100 Δcm^{-1} indicative of internal mode of phosphate were observed. Spectroscopic patterns for MFS also changed over the incubation period. The Raman spectra of MFS at early time points showed a band of ν_2 P-O stretching (1006 Δcm^{-1}), ν_1 PO_4^{3-} or P-O stretching (954 Δcm^{-1}), and small ν_7 OPO bending (534 Δcm^{-1}), consistent with the presence of dicalcium phosphate dihydrate and octacalcium [21,22]. After prolonged incubation, the ν_2 P-O stretching band (1005 Δcm^{-1}) decreased whereas the ν_1 PO_4^{3-} stretching band (961 Δcm^{-1}) was greatly increased. Moreover, ν_2 PO_4^{3-} bending (434 Δcm^{-1}), ν_3 PO_4^{3-} stretch (1041 and 1072 Δcm^{-1}), and ν_4 PO_4^{3-} bending (590 Δcm^{-1}) were observed. These spectra suggested that the majority of mineral crystals consisted of octacalcium phosphate, carbonate apatite and hydroxyapatite [21–23].

Cytotoxicity assessment

Indirect cytotoxicity measurements were performed on NIH3T3 cells at 24 and 48 h after exposing cells to different concentrations of scaffold extraction medium. The total number of cells cultured in medium extracted from FS, MFS, 0.25 g and 0.5 g nHA/FS was equivalent to those cultured in control fresh medium. Moreover, a significant difference ($p<0.05$) was observed between total number of cells exposed to extracted medium when compare to total number of cells cultured in medium extracted from latex, which is known to be toxic to the cells (data not shown). The morphology of cells was observed using phase contrast microscopy. Cells cultured in scaffold extraction medium spread, proliferated and formed monolayers comparable to cells cultured in control medium. In contrast, cells cultured in latex extraction medium appeared round in shape and were not able to proliferate (data not shown). These results suggested that the scaffolds were not toxic to NIH3T3 cells.

Calvarial cell morphology, proliferation and differentiation on fibrin-based scaffolds

SEM micrographs of primary calvarial cells cultured on different types of scaffolds are shown in Fig. 3A. A high cell density was observed on the surface of the scaffolds, indicative of

cytocompatibility. Furthermore, cells were able to adhere, spread, form cell-cell contacts, and form monolayers on all the scaffolds examined, as indicated by the flattened and polygonal morphology of the cells covering the surface of the biomaterial at 7 days. At 21 days, multiple cell layers and accumulation of fibrillar, extracellular substances were observed (Fig. 3A), suggesting that the cells could form differentiated nodules and this finding was noted as early as 14 days.

Calvarial cell proliferation increased on all scaffolds evaluated (FS, MFS, 0.25g and 0.5 g nHA/FS) from 1 day to 7 days (Fig. 3B). The total number of cells exposed to MFS, 0.25 g or 0.5 g nHA/FS was significantly ($p<0.05$) lower than FS at 1 day and 7 day. To assess affects on cell differentiation, FS, MFS, 0.25 g and 0.5 g nHA/FS scaffolds were loaded with primary calvarial cells and cultured in osteogenic medium. ALP activity was determined at 7, 14, and 21 days. MFS seeded with calvarial cells expressed higher ALP activity than FS, 0.25 g or 0.5 g nHA/FS at day 14 and 21 (Fig. 3C). A significant difference in ALP activity between MFS and FS ($p<0.05$) was noted at day 14 and 21. On the other hand, a significant difference in ALP activity between MFS and nHA/FS was observed only at day 21. In particular, ALP activity of primary calvarial cells grown on MFS increased continuously over the observation period, with significant increases ($p<0.05$) at day 21 compared to day 7 and day 14, as well as day 14 compared to day 7. For 0.25 g nHA/FS, ALP activity was significantly higher at day 21 compared to day 14. When primary calvarial cells were cultured on the scaffolds in osteogenic medium lacking β-glycerophosphate, a similar trend of ALP activity over time was observed (data not shown).

Mineralization of primary calvarial cells cultured on scaffolds was measured at day 0, 7, 14, and 21 (Fig. 3D). The calcium content of the scaffolds increased continuously over the culture period. In FS, the calcium content of primary calvarial cells cultured on scaffolds in osteogenic medium for 14 and 21 days was significant higher compared to baseline (day 0). Furthermore, the calcium content at day 21 was significantly higher compared to day 7 and day 14. On the other hand, primary calvarial cells cultured on MFS showed significantly higher calcium content at day 21 compared to baseline and day 7. Regarding the nHA/FS, the calcium content of scaffolds slightly increased over the culture period, but no significant change was noted.

To further analyze calvarial cell differentiation, RT-PCR was used to assess mRNA expression of osteoblastic markers (Fig. 4). Transcripts for ALP, BSP, OCN, COL I, CBFA1 and OSX increased with incubation time in cells exposed to all the scaffold types examined. The mRNA for all osteoblast markers at day 14 and day 21, with the exception of ALP, were higher in MFS groups than FS, 0.25 g and 0.5 g nHA/FS. However, the expression level of OCN, a marker of mature osteoblasts, was comparable between MFS and nHA/FS groups, but obviously higher than the level observed in cell within FS at day 21.

Scaffold degradation and biocompatibility

To determine stability of mineral crystals incorporated in MFS and nHA/FS, the scaffolds were incubated in PBS at 37°C up to 56 days. MFS showed significantly higher mineral crystal dissolution than nHA/FS (fig. 5A).

The ability of the scaffolds to be degraded by osteoclasts was evaluated *in vitro*. In the presence of RANKL and M-CSF, bone marrow-derived macrophages differentiated into TRAP positive multinucleated osteoclasts. Aggregation and fusion of bone marrow-derived macrophages into osteoclasts were observed by SEM (Fig. 5B). In addition, resorption pits were observed in some samples (Fig. 5B), consistent with the formation of functional osteoclasts. Thus, this treatment was used to generate bone-marrow derived osteoclasts for degradation studies described below.

Degradation kinetics in the presence of calvarial cells alone, bone marrow-derived osteoclasts alone, or a mixture of both cell types (co-cultured cells) for 14 d were similar for all scaffolds. In the presence of bone marrow derived osteoclasts, FS, MFS and 0.25g nHA/FS showed a significant decrease in dry weight at 14 days compared to scaffolds seeded with calvarial cells alone or co-cultured with osteoclasts (Fig. 5C). The calcium content of scaffolds seeded with bone marrow-derived macrophage or co-cultured cells exhibited significant differences from those seeded with primary calvarial cells (Fig. 5D). These results indicated that the fibrin matrix component as well as mineral component of these scaffolds could be degraded by the osteoclasts, *in vitro*.

Biocompatibility of the scaffolds was analyzed using subcutaneous implantation (Fig. 5E). A foreign body reaction characterized by inflammation, fibroblast infiltration, and collagen deposition was observed in response to subcutaneous implantation for 14 d. In addition, the number of multinucleated giant cells was greater on MFS and nHA/FS than those on FS. The FS scaffolds were completely degraded at 30 days following subcutaneous implantation. In contrast, the MFS and nHA/FS were still present at 30 days, although partial degradation of scaffolds was noted.

Mouse calvarial defect model for bone regeneration

To determine the ability of scaffolds to support bone regeneration, a critical size defect model in mouse calvaria was utilized. 5 mm defects were created in the mouse parietal bone, and either treated with scaffolds or left empty and examined histologically with time following injury.

As shown in Fig. 6a, empty defects lacked bony ingrowth. Only a loose, thin connective tissue was observed within the defect. Defects filled with FS scaffolds contained denser connective tissue but no obvious bone-like tissue was observed. Furthermore, FS scaffold materials were no longer present in the defect after 45 days, indicating complete degradation (Fig. 6b). MFS and nHA/FS scaffolds demonstrated areas of woven bone, mostly in the lower ventral part of the defect facing the dura mater, indicating the osteoconductive property of scaffolds. Multinucleated giant cells were found in close proximity to residual scaffold materials (Fig. 6c, 6d). Some of these cells were TRAP positive (data not shown), identifying them as osteoclasts.

Addition of rhBMP-2 significantly increased bone formation in all scaffold types (Fig. 6e, 6f, 6g). The new bone, which bridged the defect site completely, exhibited lamellar structure and a large hematopoietic stromal area. In MFS+rhBMP-2 and nHA/FS+rhBMP-2 scaffolds, new bone formation and TRAP positive multinucleated cells were observed adjacent to the residual scaffold materials (data not shown). In contrast, no residual scaffolding materials were detected in FS+rhBMP-2.

In order to compare bone regenerative capacities of the scaffolds, a semi-quantitative scoring system was utilized. As shown in Fig. 7, empty defects had no (0) or minimal (1) bone formation. The bone regeneration score improved significantly in FS, MFS or nHA/Fs scaffolds compared to an empty defect, suggesting that these scaffolds promoted calvarial bone regeneration even in the absence of rhBMP-2. Addition of rhBMP-2 greatly enhanced bone regeneration in all the scaffolds and significantly increased the bone regeneration score compared to an empty defect. Moreover, bone regeneration scores were significantly higher in rhBMP-2 treated groups compared to scaffold only groups, with one exception of nHA/FS scaffolds.

Discussion

In this study we describe the development and characterization of novel calcium phosphate/fibrin-based composite scaffolds with tightly controlled pore sizes and pore interconnections. These scaffolds were biodegradable *in vitro* and *in vivo*, and were able to support primary calvarial cell adhesion, proliferation and differentiation *in vitro*. Finally, using a critical size mouse calvarial defect model, we show that the scaffolds promoted bone regeneration that was enhanced by BMP2. Together, these data suggest that calcium/fibrin composite scaffolds could be useful as regenerative materials for repair of bone defects.

Scaffold architecture, including porosity and surface roughness, has been shown to regulate osteoblast behavior including attachment, proliferation and differentiation [24,25]. For bone tissue engineering, scaffolds should have well-controlled pore size and interconnections, and nanostructured walls that provide cells with optimal cell-substrate interactions. Various methods to fabricate three-dimensional structures have been published [26,27], however, they still have limitations in controlling scaffold structure. To address these limitations, we fabricated fibrin scaffolds with tightly control pore sizes (200–250 μm) and pore interconnections. Increasing pore size and porosity resulted in greater bone ingrowth, enhanced bone formation and lead to direct osteogenesis without osteochondral formation as reported by others [24]. However, pore sizes larger than 500 μm were associated with fibrovascular tissue formation [28]. Based on the results shown (Fig. 1), the interconnected pore structure of the fibrin scaffolds assists in both cell ingrowth and distribution within the scaffolds and thus may facilitate angiogenesis and diffusion of nutrients [29]. In addition, consistent with our previous studies [11], the fibrin scaffolds fabricated using the sphere-templating technique exhibited regular pore shape, interconnectedness and spacing. In higher magnification, polymerized fibrin fibers in the size range of 40–80 nm could be seen in the scaffold walls. We observed excellent cell adhesion, proliferation and differentiation on these surfaces, suggesting that the nanofibrillar walls facilitated cell-material interactions. This could be through improved receptor recognition of fibrillary fibrin, or by increased surface area and roughness, which have been reported to enhance osteoblast cell proliferation and differentiation [25].

Fibrin was employed in the present study as the primary scaffold matrix. It has been reported that fibrin and its degradation products induce angiogenesis [5–7], and promote cell attachment and proliferation [6,7]. Fibrin has been studied for use as a cell carrier [30], a growth factor carrier [10] and a scaffold material for bone tissue engineering [8,30]. However, it has also been reported that fibrin gels in combination with PLGA scaffolds do not enhance bone-tissue invasion into the scaffolds nor at the defect site [9]. This may be caused by the dense structural properties of the fibrin matrices that result in a reduced capacity for host tissue invasion during wound healing [9]. As shown in Fig. 5E and Fig. 6, using either subcutaneous or calvarial defect models, we were able to improve host tissue interaction by controlling architecture microporous nanofibrous fibrin scaffolds.

As presented in this study, primary calvarial cells seeded on MFS and nHA/FS exhibited lower cell proliferation compared to those seeded on non-mineralized scaffolds. These results support the data from previous studies [32,33]. There are several mechanisms to explain the decreased proliferation of osteoblast cells on MFS and nHA/FS. First, the attenuated proliferation may be caused by differentiation of cells towards the mature osteogenic phenotype similar to mesenchymal stem cells (MSC) that are known to exhibit a marked decrease in proliferation when cell differentiation is initiated [32,34]. Second, it has been reported that osteoblast-like cells isolated from rat calvaria undergo apoptosis as a fundamental component of osteoblast differentiation *in vitro* and *in vivo* [35]. Third, the low cell proliferation on calcium phosphate crystals may occur as a result of insufficient adhesion leading to poor signaling for cell cycle

progression [36]. We believe that the enhanced cell differentiation observed here is the most likely reason for the lower cell proliferation on MFS and nHA/FS vs FS scaffolds in this study. This is corroborated by the findings of a significant increase in ALP activity and increased mRNA levels for OCN, a marker of osteogenic differentiation, in cells cultured on MFS and nHA/FS vs FS scaffolds (Fig. 4).

The dissolution rate of calcium phosphate materials has been proposed as an important factor for promotion of osteogenesis [37], and mild dissolution has been noted to provide a suitable calcium and phosphate ionic environment that is needed for bone formation [37]. Rapid dissolution of the materials may be harmful and inhibit osteogenesis [37]. On the other hand, it has been reported that high extracellular calcium concentrations stimulate cell proliferation and expression of collagen and BMPs in human osteoblasts [38], whereas inorganic phosphate has been reported to upregulate osteopontin expression [39] and is proposed as a signaling molecule for osteoblast cell differentiation [40]. Moreover, inorganic phosphate upregulated genes including the SIBLING family genes; osteopontin (Opn, >300% of control) and dentin matrix protein-1 (Dmp-1, >3,000% of control) in cementoblasts [41]. Our group has previously reported that inorganic phosphate could directly stimulate human aortic smooth muscle cells to undergo an osteochondrogenic phenotypic change [42]. In the present study, we observed that MFS had a higher mineral dissolution rate than FS and nHA/FS. Primary calvarial cells seeded on MFS exhibited higher ALP activity and osteoblast marker gene expression than those of FS and nHA/FS. Together, these data suggest that the dissolution of calcium phosphate crystals leads to an increase in the concentration of calcium and phosphate ions at the local site and this promotes osteoblastic differentiation on the scaffolds. This was also suggested by the finding that the ALP activity of osteoblasts cultured on MFS in osteogenic medium without β-glycerophosphate expressed significantly higher ALP activity compared to those cultured on FS and nHA/FS.

Ideally, for clinical application in bone regeneration, scaffolds should gradually degrade and be fully replaced by natural bone tissue. In the present study, we demonstrated that FS, MFS and nHA/FS were degraded upon seeding with osteoclasts *in vitro* as well as with implantation *in vivo*. The FS scaffolds degraded completely within 30 days of subcutaneous implantation. This result corresponds to the study of Cronin KJ, et al, which showed that upon implantation of fibrin glue in a murine chamber model *in vivo*, residual fibrin was found in the two-week specimens and was completely absent in four- and six- week specimens, replaced mostly by vascularized connective tissue [43].

In this study, we observed low to moderate woven bone formation in the calvarial defect around the MFS and nHA/FS, suggesting that these materials have osteoconductive properties and may support osteogenic cell proliferation, as well as, differentiation with subsequent formation of bone matrix. The lack of a more robust response, such as that seen with addition of rhBMP-2, may be due to lack of progenitor cells or osteogenic inductive molecules within the defect area. Indeed, bone formation was significantly enhanced by addition of rhBMP-2. These results suggest that microporous nanofibrous fibrin-based scaffolds retain active rhBMP-2 and allow efficient release as well as support the biological function of rhBMP-2 *in vivo*. The rh-BMP-2 is expected to be released from FS by a simple diffusion-controlled mechanism whereas releasing of rhBMP-2 from MFS or nHA/FS may also be dependent on the crystallinity, pH, temperature, and dissolution of mineral crystals [44].

Conclusion

Polymer/calcium phosphate composite biomaterials have been proposed as candidate biomaterials for treatment of bone defects. The fibrin-based composite scaffolds described in the present study are non-toxic, biodegradable, and support cell proliferation and maturation

both *in vitro* and *in vivo*. Furthermore, these scaffolds supported bone formation in a mouse calvarial defect model. The favorable properties of these scaffolds make them excellent candidate materials for use in bone tissue engineering.

Acknowledgement

The authors gratefully acknowledge the UWEB Optical Microscopy and Image Analysis Shared Resource (NSF Grants EEC-9872882 and EEC-9529161), the UW center of Nanotechnology. This study was funded in part by the School of Dentistry Research Funding, University of Washington, NIH/NIDCR DE15109 (MS), and unrestricted funds to CG. TO is supported by a scholarship from the Anandamahidol Foundation, under the Royal Patronage of His Majesty the King of Thailand.

References

1. Yaszemski MJ, Payne RG, Hayes WC, Langer R, Mikos AG. Evolution of bone transplantation: molecular, cellular and tissue strategies to engineer human bone. Biomaterials 1996;17(2):175–185. [PubMed: 8624394]
2. Schliephake H, Tavassol F, Gelinsky M, Dard M, Sewing A, Pompe W. Use of a mineralized collagen membrane to enhance repair of calvarial defects in rats. Clin Oral Implants Res 2004;15(1):112–118. [PubMed: 14731184]
3. Kim SS, Sun Park M, Jeon O, Yong Choi C, Kim BS. Poly(lactide-co-glycolide)/hydroxyapatite composite scaffolds for bone tissue engineering. Biomaterials 2006;27(8):1399–1409. [PubMed: 16169074]
4. Athanasiou KA, Niederauer GG, Agrawal CM. Sterilization, toxicity, biocompatibility and clinical applications of polylactic acid/polyglycolic acid copolymers. Biomaterials 1996;17(2):93–102. [PubMed: 8624401]
5. Takei A, Tashiro Y, Nakashima Y, Sueishi K. Effects of fibrin on the angiogenesis in vitro of bovine endothelial cells in collagen gel. In Vitro Cell Dev Biol Anim 1995;31(6):467–472. [PubMed: 8589891]
6. Bootle-Wilbraham CA, Tazzyman S, Thompson WD, Stirk CM, Lewis CE. Fibrin fragment E stimulates the proliferation, migration and differentiation of human microvascular endothelial cells in vitro. Angiogenesis 2001;4(4):269–275. [PubMed: 12197472]
7. Herrick S, Blanc-Brude O, Gray A, Laurent G. Fibrinogen. Int J Biochem Cell Biol 1999;31(7):741–746. [PubMed: 10467729]
8. Jegoux F, Goyenvalle E, Bagot D'arc M, Aguado E, Daculsi G. In vivo biological performance of composites combining micro-macroporous biphasic calcium phosphate granules and fibrin sealant. Arch Orthop Trauma Surg 2005;125(3):153–159. [PubMed: 15761734]
9. Karp JM, Sarraf F, Shoichet MS, Davies JE. Fibrin-filled scaffolds for bone-tissue engineering: An in vivo study. J Biomed Mater Res A 2004;71(1):162–171. [PubMed: 15368266]
10. Schmoekel HG, Weber FE, Schense JC, Gratz KW, Schawalder P, Hubbell JA. Bone repair with a form of BMP-2 engineered for incorporation into fibrin cell ingrowth matrices. Biotechnol Bioeng 2005;89(3):253–262. [PubMed: 15619323]
11. Linnes MP, Ratner BD, Giachelli CM. A fibrinogen-based precision microporous scaffold for tissue engineering. Biomaterials 2007;28(35):5298–5306. [PubMed: 17765302]
12. Tarasevich BJCC, Allara DL. Nucleation and growth of calcium phosphate from physiological solutions onto self-assembled templates by a solution-formed nucleus mechanism. J Phys Chem B 2003;107:10367–10377.
13. Zhou H, Mak W, Zheng Y, Dunstan CR, Seibel MJ. Osteoblasts directly control lineage commitment of mesenchymal progenitor cells through WNT signaling. J Biol Chem. 2007
14. Datta NS, Chen C, Berry JE, McCauley LK. PTHrP signaling targets cyclin D1 and induces osteoblastic cell growth arrest. J Bone Miner Res 2005;20(6):1015–1064.
15. Cowan CM, Shi YY, Aalami OO, Chou YF, Mari C, Thomas R, et al. Adipose-derived adult stromal cells heal critical-size mouse calvarial defects. Nat Biotechnol 2004;22(4):560–567. [PubMed: 15077117]

16. Itaka K, Ohba S, Miyata K, Kawaguchi H, Nakamura K, Takato T, et al. Bone regeneration by regulated in vivo gene transfer using biocompatible polyplex nanomicelles. Mol Ther 2007;15(9): 1655–1662. [PubMed: 17551504]

17. Hirata K, Tsukazaki T, Kadowaki A, Furukawa K, Shibata Y, Moriishi T, et al. Transplantation of skin fibroblasts expressing BMP-2 promotes bone repair more effectively than those expressing Runx2. Bone 2003;32(5):502–512. [PubMed: 12753866]

18. Mankani MH, Kuznetsov SA, Avila NA, Kingman A, Robey PG. Bone formation in transplants of human bone marrow stromal cells and hydroxyapatite-tricalcium phosphate: prediction with quantitative CT in mice. Radiology 2004;230(2):369–376. [PubMed: 14752182]

19. Nancollas GH. The involvement of calcium phosphate in biological mineralization and demineralization processes. Pure&Appl Chem 1992;64(11):1673–1678.

20. Cheng PT. Formation of octacalcium phosphate and subsequent transformation to hydroxyapatite at low supersaturation: a model for cartilage calcification. Calcif Tissue Int 1987;40(6):339–343. [PubMed: 3038281]

21. Taddei PTA, Bottura G, Bertoluzza A. Vibration spectroscopic characterization of new calcium phosphate bioactive coating. Biopolymers (Biospectroscopy) 2000;57

22. Fowler BOMM, Brown WE. Octacalcium phosphate. 3. Infrared and Raman vibrational spectra. Chem Mater 1993;5:1417–1423.

23. Crane NJ, Popescu V, Morris MD, Steenhuis P, Ignelzi MA Jr. Raman spectroscopic evidence for octacalcium phosphate and other transient mineral species deposited during intramembranous mineralization. Bone 2006;39(3):434–442. [PubMed: 16627026]

24. Karageorgiou V, Kaplan D. Porosity of 3D biomaterial scaffolds and osteogenesis. Biomaterials 2005;26(27):5474–5491. [PubMed: 15860204]

25. Lincks J, Boyan BD, Blanchard CR, Lohmann CH, Liu Y, Cochran DL, et al. Response of MG63 osteoblast-like cells to titanium and titanium alloy is dependent on surface roughness and composition. Biomaterials 1998;19(23):2219–2232. [PubMed: 9884063]

26. Liu X, Ma PX. Polymeric scaffolds for bone tissue engineering. Ann Biomed Eng 2004;32(3):477–486. [PubMed: 15095822]

27. Hutmacher DW. Scaffold design and fabrication technologies for engineering tissues--state of the art and future perspectives. J Biomater Sci Polym Ed 2001;12(1):107–124. [PubMed: 11334185]

28. Wake MCPC, Mikos AG. Pore morphology effects on the fibrovascular tissue growth in porous polymer substrates. Cell Transplantation 1994;3(4):339–343. [PubMed: 7522866]

29. Salgado AJ, Coutinho OP, Reis RL. Bone tissue engineering: state of the art and future trends. Macromol Biosci 2004;4(8):743–765. [PubMed: 15468269]

30. Boo JS, Ozawa R, Nagasaka T, Okazaki Y, Hata K, et al. Bone regeneration following injection of mesenchymal stem cells and fibrin glue with a biodegradable scaffold. J Craniomaxillofac Surg 2003;31(1):27–33. [PubMed: 12553923]

31. Le Guehennec L, Goyenvalle E, Aguado E, Pilet P, Bagot D'Arc M, Bilban M, et al. MBCP biphasic calcium phosphate granules and tissucol fibrin sealant in rabbit femoral defects: the effect of fibrin on bone ingrowth. J Mater Sci Mater Med 2005;16(1):29–35. [PubMed: 15754141]

32. Niemeyer P, Krause U, Fellenberg J, Kasten P, Seckinger A, Ho AD, et al. Evaluation of mineralized collagen and alpha-tricalcium phosphate as scaffolds for tissue engineering of bone using human mesenchymal stem cells. Cells Tissues Organs 2004;177(2):68–78. [PubMed: 15297781]

33. Siebers MC, Walboomers XF, Leeuwenburgh SC, Wolke JG, Jansen JA. The influence of the crystallinity of electrostatic spray deposition-derived coatings onosteoblast-like cell behavior, in vitro. J Biomed Mater Res A 2006;78(2):258–267. [PubMed: 16628711]

34. Uebersax L, Hagenmuller H, Hofmann S, Gruenblatt E, Muller R, Vunjak-Novakovic G, et al. Effect of scaffold design on bone morphology in vitro. Tissue Eng 2006;12(12):3417–3429. [PubMed: 17518678]

35. Lynch MP, Capparelli C, Stein JL, Stein GS, Lian JB. Apoptosis during bone-like tissue development in vitro. J Cell Biochem 1988;68(1):31–49. [PubMed: 9407312]

36. Lee YJ, Ko JS, Kim HM. The role of cell signaling defects on the proliferation of osteoblasts on the calcium phosphate apatite thin film. Biomaterials 2006;27(20):3738–3744. [PubMed: 16530826]

37. Yuan H, Yang Z, Li Y, Zhang X, De Bruijn JD, De Groot K. Osteoinduction by calcium phosphate biomaterials. J Mater Sci Mater Med 1998;9(12):723–726. [PubMed: 15348929]

38. Nakade O, Takahashi K, Takuma T, Aoki T, Kaku T. Effect of extracellular calcium on the gene expression of bone morphogenetic protein-2 and -4 of normal human bone cells. J Bone Miner Metab 2001;19(1):13–19. [PubMed: 11156467]

39. Beck GR Jr, Knecht N. Osteopontin regulation by inorganic phosphate is ERK1/2-, protein kinase C-, and proteasome-dependent. J Biol Chem 2003;278(43):41921–41929. [PubMed: 12920127]

40. Beck GR Jr. Inorganic phosphate as a signaling molecule in osteoblast differentiation. J Cell Biochem 2003;90(2):234–243. [PubMed: 14505340]

41. Foster BL, Nociti FH Jr, Swanson EC, Matsa-Dunn D, Berry JE, Cupp CJ, et al. Regulation of cementoblast gene expression by inorganic phosphate in vitro. Calcif Tissue Int 2006;78(2):103–112. [PubMed: 16467974]

42. Jono S, McKee MD, Murry CE, Shioi A, Nishizawa Y, Mori K, et al. Phosphate regulation of vascular smooth muscle cell calcification. Circ Res 2000;87(7):E10-7. [PubMed: 11009570]

43. Cronin KJ, Messina A, Thompson EW, Morrison WA, Stevens GW, Knight KR. The role of biological extracellular matrix scaffolds in vascularized three-dimensional tissue growth in vivo. J Biomed Mater Res B Appl Biomater 2007;82(1):122–118. [PubMed: 17106890]

44. Kim SS, Gwak SJ, Kim BS. Orthotopic bone formation by implantation of apatite-coated poly(lactide-co-glycolide)/hydroxyapatite composite particulates and bonemorphogenetic protein-2. J Biomed Mater Res A. 2008

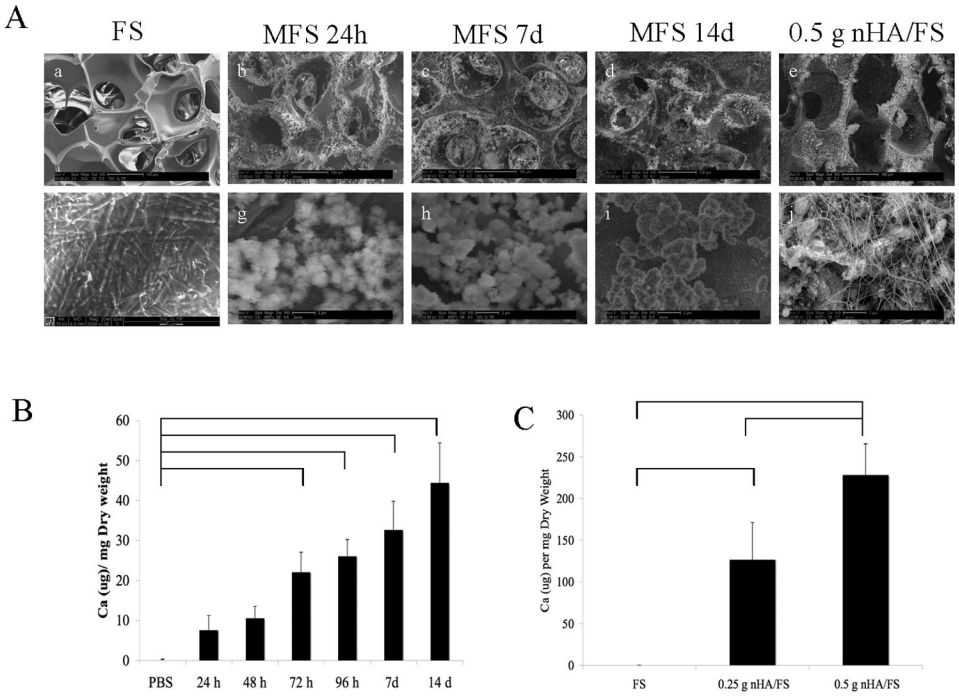

Figure 1.

(A) SEM micrographs illustrating the surface structure of microporous nanofibrous fibrin scaffolds. (a) Fibrin scaffolds (FS) in PBS for 14 d; (b–d) Mineralized fibrin scaffolds (MFS) in saturated calcium phosphate solution for 24h, 7d and 14 d, respectively; (e) Representative structure of nanocrystal-incorporated hydroxyapatite fibrin scaffolds (nHA/FS, 0.5 g). Higher magnification SEM micrographs to clarify the mineral crystal structure is shown in (f–j). (B) The quantification of calcium content in the Mineralized fibrin scaffolds (MFS) in saturated calcium phosphate solution for various time points. (C) The quantification of calcium content of nanocrystal-incorporated hydroxyapatite fibrin scaffolds (nHA/FS, 0.25 g and 0.5 g) compare to Fibrin scaffolds (FS).

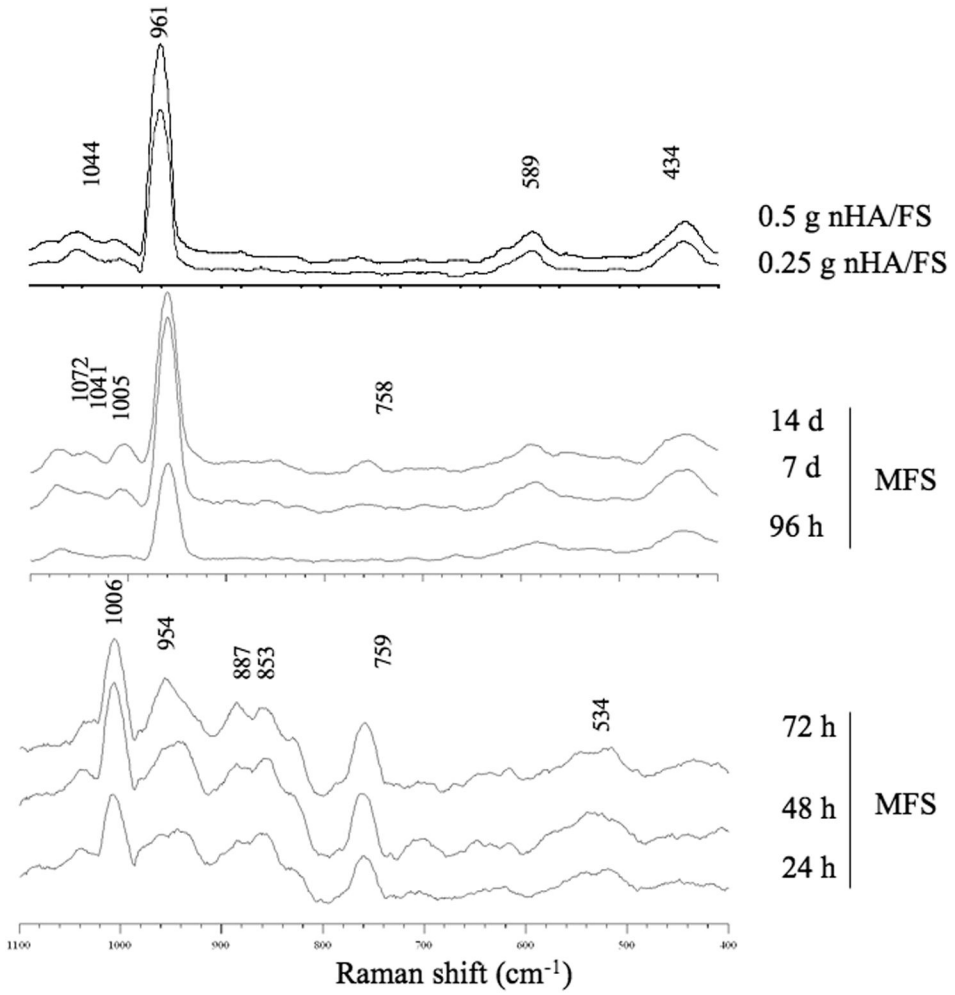

Figure 2.

Raman spectra focused on the phosphate's internal mode, the 400–1100 Δcm^{-1} range of mineralized fibrin scaffolds (MFS) incubated in saturated calcium phosphate solution and nanocrystal incorporated hydroxyapatite fibrin scaffolds (nHA/FS).

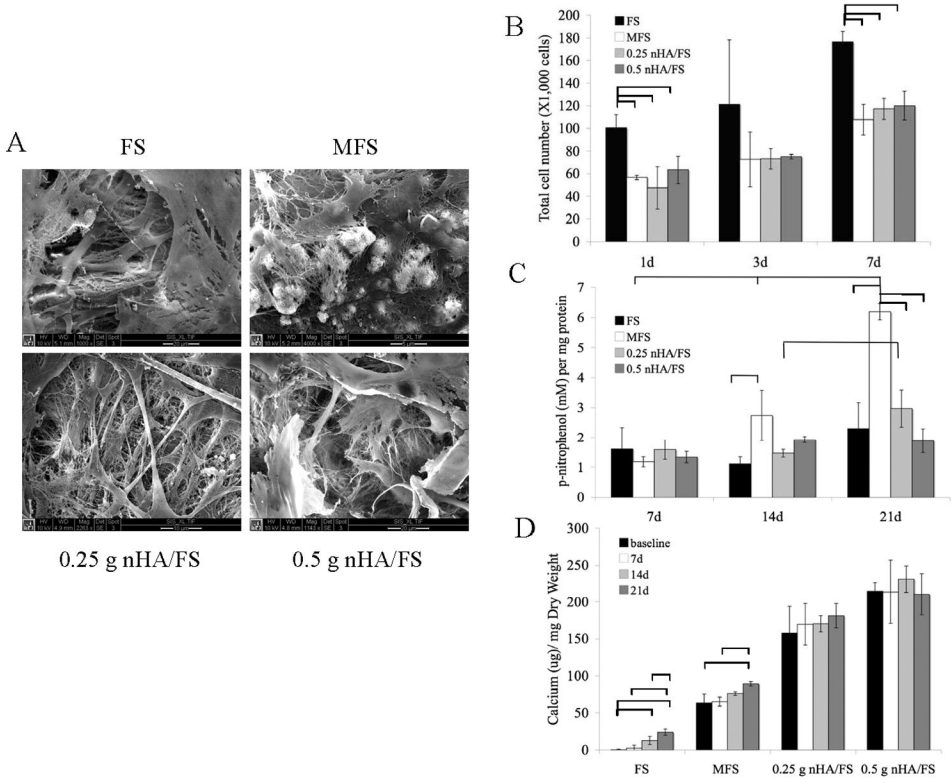

Figure 3.

(A) SEM showing the surface of fibrin scaffolds (FS), mineralized fibrin scaffolds (MFS), 0.25 g nanocrystal incorporated hydroxyapatite fibrin scaffolds (nHA/FS) and 0.5 g nanocrystal incorporated hydroxyapatite fibrin scaffolds (nHA/FS) after seeding with primary calvarial cells for 21 days. (B) Proliferation of primary calvarial cells on fibrin-based scaffolds. (C) Alkaline phosphatase activity of primary calvarial cells cultured on fibrin-based scaffolds in osteogenic medium. (D) Mineral deposition of primary calvarial cells on fibrin-based scaffolds. The bars indicate statistical significance at $p<0.05$.

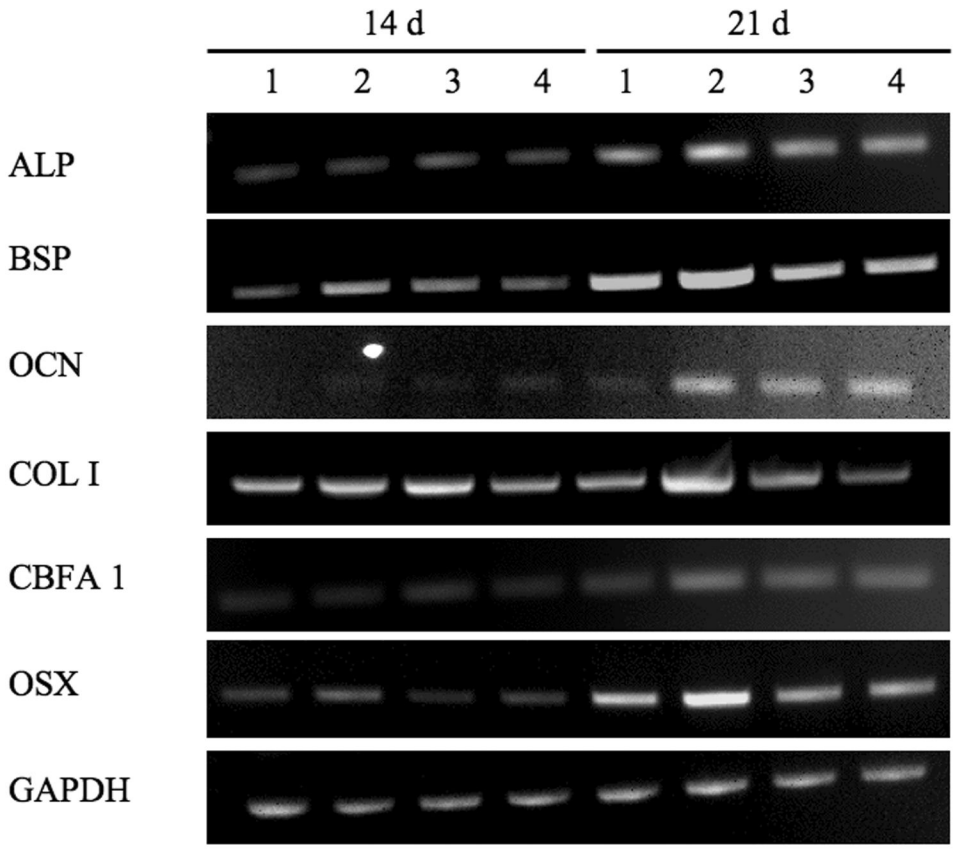

Figure 4.
Osteoblast marker gene expression of primary calvarial cells cultured on the scaffolds in osteogenic medium for 14 and 21 d. lane 1: fibrin scaffolds (FS); lane 2: mineralized fibrin scaffolds (MFS); lane 3: 0.25 g nanocrystal incorporated hydroxyapatite fibrin scaffolds (nHA/FS); lane 4: 0.5 g nanocrystal incorporated hydroxyapatite fibrin scaffolds (nHA/FS).

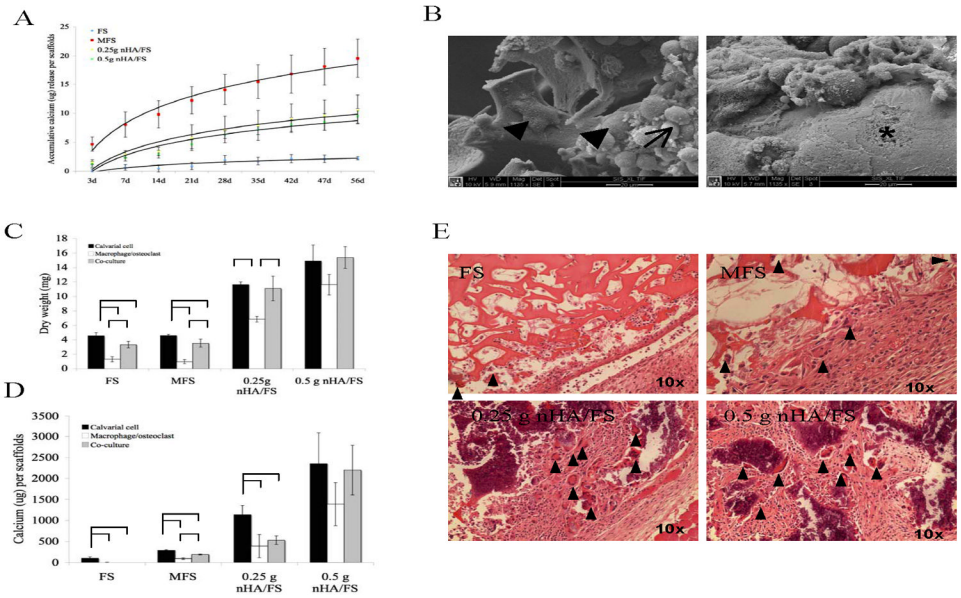

Figure 5.

(A) The dissolution of mineral crystals from fibrin-based scaffolds incubated in PBS at 37°C. (B) SEM showing the morphology of bone marrow-derived macrophage cells alone cultured on fibrin scaffolds (supplement with M-CSF and RANKL). The cell fusion (arrow head), cell aggregation (arrow) and resorption pit (asterix) are shown. For the cell mediated degradation study, scaffolds were seeded with primary calvarial cells, bone marrow-derived macrophages or co-culture. The dry weight (C) and calcium content (D) of scaffolds were measured. (E) Histological images of subcutaneously implanted scaffolds for 14 days. Arrowheads show the multinucleated giant cells.

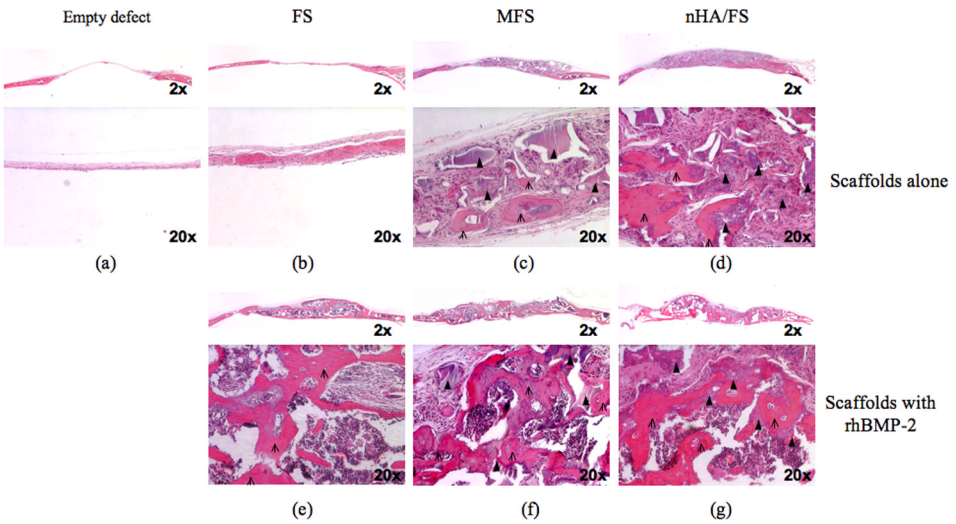

Figure 6.

Representative low and high magnification histological images of mouse calvarial defects at 45 days after surgery. The empty defects are shown in column 1. Defects were treated with fibrin scaffolds (FS: column 2), mineralized fibrin scaffolds (MFS: column 3), and 0.5 g nanocrystal incorporated hydroxyapatite fibrin scaffolds (nHA/FS: column 4). For each type of scaffolds, treatments were divided into two groups; 1) scaffolds alone (upper row), 2) scaffolds+rhBMP-2 (lower row). Arrows represent the remaining scaffolds and open arrows represent bone tissue formation.

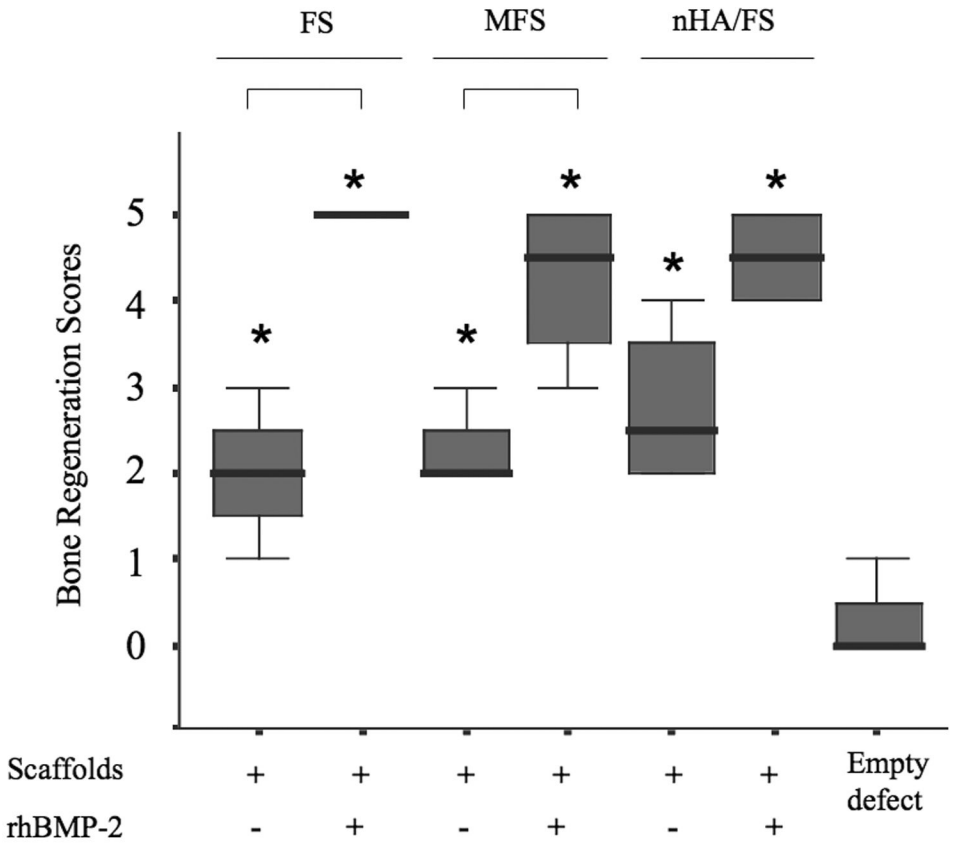

Figure 7.

Semi-quantitative scores of bone regeneration in the calvarial defects are presented as box plots, where the boxes represent the first and third quartiles. The line in the box represents the median and lines outside the box represent the spread of values. Asterix (*) shows the significant at $p<0.05$ compared to the empty defect. Bars show the significant difference between groups ($p<0.05$).

Table 1

Semi-quantitative scoring parameters for evaluation of bone regeneration.

Score	Extent of Bone in Defect
0	No bone formation
1	Minimal bone formation (one very small area in the defect)
2	Low bone formation, occupying only small portion of the defect
3	Moderate bone formation, occupying substantial portion but less than three quarter of the defect
4	Abundant bone formation, occupying greater than three quarter of the defect
5	Complete mature bone formation, occupying greater than three quarter of the defect with obvious abundant mature marrow cavity

Modified from Mankani M, et al.

Table 2

Atomic Ca/P ratio of mineralized fibrin scaffolds (MFS) incubated in saturated calcium phosphate solution over 14 days and nanocrystal incorporated hydroxyapatite fibrin scaffolds (nHA/FS).

Incubation time	Atomic Ca/P ratio range
24h	1.09–2.62
48h	1.04–1.55
72h	1.00–1.30
96h	1.12–1.77
7d	1.21–1.70
14d	1.11–1.79
0.25 g nHA/FS	1.33–1.65
0.5 g nHA/FS	1.34–1.69